



Transport variability of the Deep Western Boundary Current and the Antilles Current off Abaco Island, Bahamas

Christopher S. Meinen^{a,*}, Silvia L. Garzoli^b, William E. Johns^c,
Molly O. Baringer^b

^a*Cooperative Institute for Marine and Atmospheric Studies, University of Miami, NOAA/AOML/PHOD, 4301 Rickenbacker Causeway, Miami FL 33149, USA*

^b*Atlantic Oceanographic and Meteorological Laboratory, National Oceanic and Atmospheric Administration, Miami FL 33149, USA*

^c*Rosenstiel School of Marine and Atmospheric Science, University of Miami, Miami FL 33149, USA*

Received 30 September 2003; received in revised form 6 July 2004; accepted 15 July 2004

Available online 15 September 2004

Abstract

Hydrography is combined with 1-year-long Inverted Echo Sounder (IES) travel-time records and bottom pressure observations to estimate the Deep Western Boundary Current (DWBC) transport east of Abaco Island, the Bahamas (near 26.5°N); comparison of the results to a more traditional line of current meter moorings demonstrates that the IESs and pressure gauges, combined with hydrography, can accurately monitor the DWBC transport to within the accuracy of the current meter array estimate at this location. Between 800 and 4800 dbar, bounded by two IES moorings 82 km apart, the enclosed portion of the DWBC is shown to have a mean southward transport of about 25 Sv (1 Sv = 10⁶ m³ s⁻¹) and a standard deviation of 23 Sv. The DWBC transport is primarily barotropic (where barotropic is defined as the near-bottom velocity rather than the vertical average velocity); geostrophic transports relative to an assumed level of no motion do not accurately reflect the actual absolute transport variability (correlation coefficient is 0.30). The IES-pressure gauge absolute transport within 1200–4800 dbar agrees well with the current meter absolute transports (upper integration limit based on shallowest current meter level); the standard deviation of the difference is 12 Sv and the mean difference is 0.2 Sv. The correlation coefficient between these two time series is 0.76. The northward flowing Antilles Current (AC) east of Abaco Island has a mean baroclinic transport of 6 Sv as estimated by the IESs and a standard deviation of 3 Sv. The AC variations observed during 1996–1997 are uncorrelated with the Florida Current transport variations west of Abaco Island in the Florida Straits, however, the AC transport variations bear some resemblance to the historical estimates of the AC annual cycle.

© 2004 Elsevier Ltd. All rights reserved.

*Corresponding author. Tel.: +1-305-361-4355; fax: +1-305-361-4412.

E-mail addresses: christopher.meinen@noaa.gov (C.S. Meinen), silvia.garzoli@noaa.gov (S.L. Garzoli), wjohns@rsmas.miami.edu (W.E. Johns), molly.baringer@noaa.gov (M.O. Baringer).

1. Introduction

A significant fraction, albeit definitely not all, of the deep water masses in the world ocean are believed to have last interacted with the ocean surface when they were in the northern Atlantic Ocean. The meridional overturning cell (MOC) that moves these deep waters around the world is not a stationary system, with changes occurring in the area of deep water formation and in the amount of deep water exported from the northern North Atlantic along the western boundary (Dickson et al., 2002; Schott et al., 2004). The picture is further complicated because the pathway for deep water flow is not as simple as was once thought, with some observations and models indicating that the deep outflow from the northern North Atlantic can occur away from the western boundary in the interior (Smethie et al., 2000; Schott et al., 2004) and studies using subsurface floats and tracer hydrography suggest that the deep flow along the western boundary of the Atlantic near Canada may not continue southward along the boundary beyond the Southeast Newfoundland Rise (Fischer and Schott, 2002; Rhein et al., 2002).

The path of the Deep Western Boundary Current (DWBC) in the subtropical Atlantic has been studied extensively; the DWBC meanders and bifurcates under the Gulf Stream (Pickart, 1994) and then continues southward to the east of the Bahamas (Johns et al., 1997). Several long-term mooring arrays have been placed along the DWBC path to investigate the spatial and temporal variability of the flow: for example, near the Southeast Newfoundland Ridge (Schott et al., 2004), east of the Bahamas (Lee et al., 1996) and in the equatorial Atlantic (Fischer and Schott, 1997). The longest time series of moored and hydrographic observations has been at roughly 26.5°N, east of Abaco Island, the Bahamas (Molinari et al., 1998). Current meter studies at 26.5°N have shown that the southward flowing DWBC has a mean transport of 40 Sv ($1 \text{ Sv} = 10^6 \text{ m}^3 \text{ s}^{-1}$), although as much as 27 Sv of that may be recirculating to the north within the interior of the basin (Lee et al., 1996). East of Abaco the DWBC is overlaid by the northward flowing

Antilles Current (AC) in the upper 800–1000 m; the AC has a mean transport of about 5 Sv (e.g. Lee et al., 1996). The DWBC and AC have been shown to vary on annual and semiannual time scales (e.g. Rosenfeld et al., 1989).

Study of the deep branch of the MOC is complicated and expensive due to the presence of surface currents (e.g. AC, Gulf Stream, North Atlantic Current), varying pathways and significant recirculations. One fact that is quite evident is that an efficient and inexpensive method for observing/monitoring the MOC flows is needed. Arrays involving large numbers of moorings with multiple current meters are not financially practical for spanning large portions of the basin over periods of many years to quantify the MOC flow and its variability. The purpose of this paper is twofold. First, to investigate the feasibility of quantifying the DWBC transport using a combination of inverted echo sounders (IESs) and deep pressure gauges by comparing the results to those from a concurrent line of traditional current meter moorings at 26.5°N off Abaco Island in the Bahamas. The second purpose is to present the time variability of both the DWBC and the shallow northward flowing AC for the period July 1996–June 1997 and discuss these results in the wider context of the flow throughout the region.

2. Data

Four primary instrument data sets are used in this analysis; conductivity–temperature–depth (CTD) profilers, deep pressure gauges, current meter moorings (CMMs), and IESs. The CMMs and IESs were deployed in a line eastward along 26.5°N from Abaco Island in the Bahamas (Fig. 1) from October 1995 to June 1997 and from July 1996 to June 1997, respectively. A complete description of the moored current meter results can be found in Zantopp et al. (1998) and Johns et al. (submitted for publication); the latter also presents a comparison between current meter-derived transports to transports derived from dynamic height mooring data. In this paper, the current meter data are used only to compare with

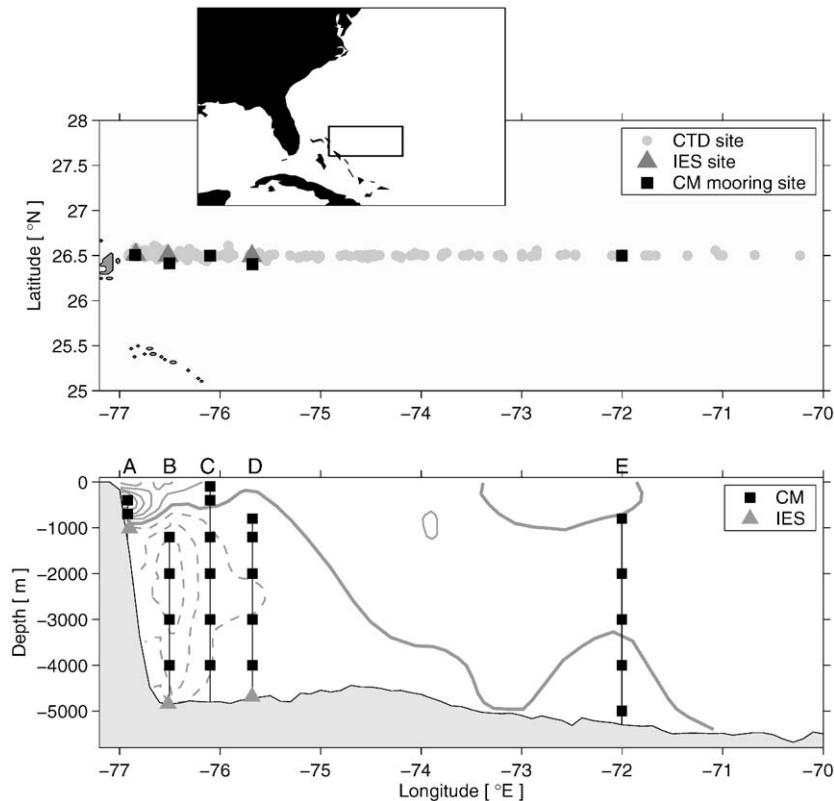


Fig. 1. Location of the moored instruments and CTD observations used in this study. Small inset panel indicates study area relative to the North American continent. Lower panel shows the vertical distribution of instruments, with bottom topography from the Smith and Sandwell (1997) dataset indicated in gray. Contours indicate the average meridional velocity from 11 CTD/Pegasus sections as presented in Lee et al. (1990); solid and dashed contours indicate 5 cm s^{-1} positive and negative intervals, respectively, while bold solid contour indicates zero flow.

the IES-derived quantities. One CMM (site A) was deployed on the shelf in about 1000 m of water with an IES located nearby ($<5 \text{ km}$); the remaining CMMs and IESs were deployed in deep water at varying distances from the shelf (Fig. 1, lower panel). Mooring sites B, C, and D were chosen to span the location of the core of the DWBC based on previous studies (Leaman and Harris, 1990; Lee et al., 1996), while site E was chosen to sample the flows further offshore. Site A was occupied in order to measure the shallow northward flowing current, often called the Antilles Current (AC, e.g. Lee et al., 1990; Leaman and Harris, 1990). Each of the four deep CMMs was additionally equipped with a bottom pressure gauge at the base of each mooring.

Two-hundred sixty CTD casts were obtained along the Abaco region during the period 1985–2002 (Fig. 1); of these, 229 reached at least 3000 dbar ($1 \text{ dbar} = 10^4 \text{ Pa}$) and an additional 22 reached at least 1000 dbar. The CTD casts were acquired fairly evenly over the 18 year period, and they were spread fairly evenly throughout the year except for November and December, when few observations were made. In Section 3, how these hydrography measurements were used to develop the empirical characteristic relationships needed to analyze the IES measurements is discussed.

An IES is about 0.6-m tall and is moored roughly 1 m off the ocean bottom. It transmits a 10 kHz sound pulse and measures the time (τ) for the pulse to travel to the ocean surface and back

(Watts and Rossby, 1977; Chaplin and Watts, 1984). The raw IES records were first filtered with a 40 h boxcar filter to remove most of the tidal signal. IES and CMM data were also subsampled from their original hourly sampling rate down to

once per day, at noon GMT. Finally, all time series presented herein have been smoothed with a 5-day running-mean to remove higher-frequency signals.

3. Methods

All analyses of IES data depend upon empirical characteristic relationships determined independently from hydrography. The data from CTD casts are used to simulate the travel time that would be measured at any depth z by using the measured temperature (T) and salinity (S) along with the empirical equation for sound speed in water, $c(S, T, p)$, via the following equation:

$$\tau_{\text{sim}} = 2 \int_z^0 \frac{1}{c} dz', \quad (1)$$

where τ_{sim} is the simulated travel time and c is calculated via the sound speed equation of Del Grosso (1974). With a τ_{sim} value associated with each CTD profile, it is possible to consider the relationships between τ_{sim} and the directly measured values of T and S from the CTD casts.

The earliest IES deployments were made in and near the Gulf Stream, where empirical relationships between τ_{sim} and the depth of the 12 °C or 15 °C isotherm were used to estimate thermocline depth from IES measurements (e.g. Rossby, 1969; Watts and Rossby, 1977; Watts et al., 1995). In recent years, empirical hydrographic relationships have been developed which can be combined with

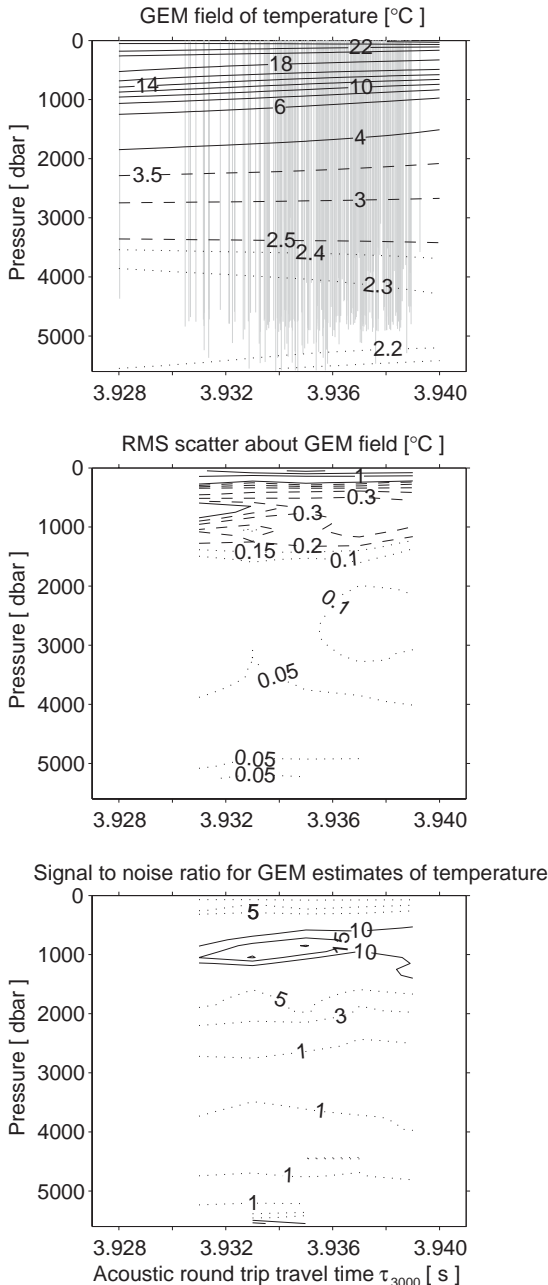


Fig. 2. Upper panel: GEM representation of temperature for the Abaco region. GEM field calculated using the data from the 229 CTD casts obtained along the Abaco line. Solid, dashed, and dotted contours denote intervals of 2, 0.5, and 0.1 °C, respectively. Vertical gray lines indicate CTD observations. Middle panel: Root-mean-squared (RMS) difference between the CTD measured T values and the temperatures which would be predicted based on the CTD τ_{sim} value and the T GEM field. Solid, dashed, and dotted contours denote intervals of 0.5, 0.1, and 0.05 °C, respectively. Bottom panel: Signal-to-noise ratio of the observed peak-to-peak signal at each depth (from top panel) to the RMS scatter at each depth (from middle panel). Solid contours are at intervals of 5, dotted contours are at intervals of 2.

the IES measured τ to estimate full water column profiles of T , S , and specific volume anomaly δ (Meinen and Watts, 2000). These relationships are referred to as the ‘Gravest Empirical Modes’, or GEMs, with separate GEM look-up tables for T , S , and δ . Vertical integration of the δ profiles yields profiles of geopotential height anomaly, which when differenced horizontally between neighboring IESs yield profiles of the relative velocity using the geostrophic (dynamic) method. This combination of hydrography-based GEM relationships and IES measurements has been successfully applied in a wide range of locations in different ocean regions, including the North Atlantic Current (Meinen and Watts, 2000), the Kuroshio (Book et al., 2002), and the Antarctic Circumpolar Current (Watts et al., 2001b; Meinen et al., 2002; Meinen and Luther, 2003). The results presented herein utilize both the simple earlier type of technique for analyzing IES data and the newer, more involved, GEM technique. Both methods depend on the availability of sufficient hydrography to characterize the suite of variability observed in the region of interest.

Before continuing, a few words are in order regarding the long term use of IESs for ocean monitoring. The empirical relationships used in analyzing the IES data may change over long time scales (decades and longer) as T – S properties change. Meinen and Watts (2000) tested the impact of using hydrography from the 1990s to build GEM fields of temperature and specific volume anomaly versus using data from the 1960s–1980s and found little difference in the resulting GEM fields. This result, however, only applies to the region studied by Meinen and Watts (the North Atlantic Current region near 42°N). Employing IESs in a long-term monitoring situation will always require occasional (every 1–2 years) hydrographic observations to test for long-term trends in the empirical relationships.

3.1. Multiple parameter relationship: obtaining DWBC transport

As mentioned earlier, hydrography can be used in combination with an IES to provide a time

series of full water column profiles of T , S , and δ (Meinen and Watts, 2000; Watts et al., 2001b). Basically, the τ_{sim} values calculated using each of the CTD casts are used to sort the T values, for example, as a function of τ_{sim} and pressure p . Smoothing splines are used to extract a look-up table of T on a regular grid of τ_{sim} and p . Fig. 2 shows the T GEM field determined from the 229 deep CTD casts, where the CTD τ_{sim} values were calculated between the surface and 3000 dbar. Prior to combining the IES time series of τ with the GEM fields such as that shown in Fig. 2 they must first be ‘calibrated’ into time series of τ_{3000} (i.e. the travel time which would have been measured at 3000 dbar if the IESs were at that level). This calibration was completed using CTDs which were taken at the IES sites during the year-long deployment. The calibration was done as follows; the IES measured τ coincident to the CTD profile time was subtracted from each day of the time series of τ for that IES, and then the CTD measured τ_{3000} was added to the full time series.¹ This ‘calibration’ is valid because τ variations are highly correlated in the vertical, with a slope that varies from one by only a few percent as a function of pressure, for depths below the main thermocline (e.g. Meinen and Watts, 1998). Once the IES-measured τ records are calibrated into τ_{3000} (only possible at sites B and D as the ‘calibration CTD’ at site A only reached about 1000 dbar due to the ocean depth at that location), the timeseries of τ_{3000} at each IES site are combined with the GEM field shown in Fig. 2 to produce a time series of full-water-column T profiles. Similar GEM fields were created for S and δ (not shown), allowing for the calculation of T , S , and δ profiles at sites B and D. Profiles of δ were vertically integrated to obtain profiles of geopotential anomaly (Φ) via the standard method;

$$\Phi = \int_0^p \delta \, dp'. \quad (2)$$

¹When multiple CTDs are available at an IES site, as is common for most deployments, they can all be used to provide a calibration via this method and the resulting time series can be averaged to yield a more accurately calibrated time series.

3.2. Absolute referencing of the geostrophic velocities

Differencing the Φ profiles at sites B and D results in a time series of estimates of the geostrophic relative velocity perpendicular to the line between sites B and D. These velocities are, of course, relative to an assumed level of no motion as are all geostrophic velocities determined via the dynamic method. The common choice of a level of no motion for this region is 800 dbar, based on previous long-term absolute velocity observations from current meters (Lee et al., 1990, 1996) and PEGASUS sections (Leaman and Harris, 1990). It will be shown, however, that applying such an assumption to the data would lead to radically inaccurate estimates of the deep transport in this region. Rather than depend on a level of no motion assumption, the IES–GEM velocities were combined with bottom pressure gauge data obtained at the same time in order to determine absolute velocity profiles.

It is well known that the horizontal gradients between pairs of deep pressure gauges are proportional to the deep absolute velocity. One well-known problem in using deep pressure gradients in this manner, however, is that the instruments cannot be geodetically leveled accurately enough to discriminate between the non-dynamical geographic pressure difference and the dynamical time-mean pressure offset associated with the deep mean geostrophic flows. As such, the gradient between instruments cannot provide an estimate of the time-mean deep velocity (Watts et al., 2001a). They can, nonetheless, provide an estimate of the absolute velocity variability. The measurements of the bottom pressure gauges at the bases of the CMMs at sites B and D were differenced and scaled by the Coriolis parameter to provide a time series of the velocity variability between the two sites via geostrophy. The time-mean deep velocity was estimated by using the time-mean meridional velocity from the 4000 dbar current meter on the mooring at site C, 8.7 cm s^{-1} . This value is very close to the 8 cm s^{-1} average determined from two LADCP sections obtained during the experiment (Johns et al., submitted for publication).

The DWBC transport is defined for the purposes of this paper as the flow between 800 and 4800 dbar. The transport is observed within the gap between the two fixed moorings at sites B and D (see Fig. 1), although transport outside this gap is discussed later as well.

3.3. Single parameter relationship: obtaining upper ocean baroclinic transport

The AC is mostly confined to the upper 800 m of the ocean, with a velocity core near 400 m, and inshore of site B (Lee et al., 1996). In addition to calculating τ_{sim} , the T and S measurements from the CTD casts can also be used to calculate the potential energy anomaly, sometimes called the Fofonoff potential (Fofonoff, 1962), between the ocean surface and 800 dbar. Fofonoff potential, χ , is determined via the following equation:

$$\chi = \frac{1}{g} \int_0^p p' \delta dp', \quad (3)$$

where g is gravity and p is pressure.² Horizontal differences of χ give the baroclinic transport within the integration layer (transport = $(\rho f)^{-1}(\chi_2 - \chi_1)$, Fofonoff, 1962).³ Therefore by developing a relationship between τ_{sim} and χ , the IES observations can be used to estimate the geostrophic transport within the upper 800 dbar relative to an assumed level of no motion at 800 dbar.

When data from each of the 251 CTD casts which reached 1000 dbar (Fig. 1) is used to calculate the Fofonoff potential above 800 dbar (χ_{800}) and the simulated travel time above 1000 dbar (τ_{1000}), the close relationship between the two quantities is clearly evident (Fig. 3). We cannot directly apply the linear fit from Fig. 3 to the IES records. Just as for the calibration of τ_{3000} discussed above for the GEM method, the IES time series of τ must be ‘calibrated’ into a time series of τ_{1000} (the travel time which would have been measured at 1000 dbar if the IESs were at

²Comparing Eqs. (2) and (3) shows that χ is roughly equivalent to the vertical integration of Φ .

³Note that χ as derived here is only the equivalent of baroclinic streamfunction when the integration limits are the ocean surface and the geostrophic reference layer (Sun and Watts, 2002).

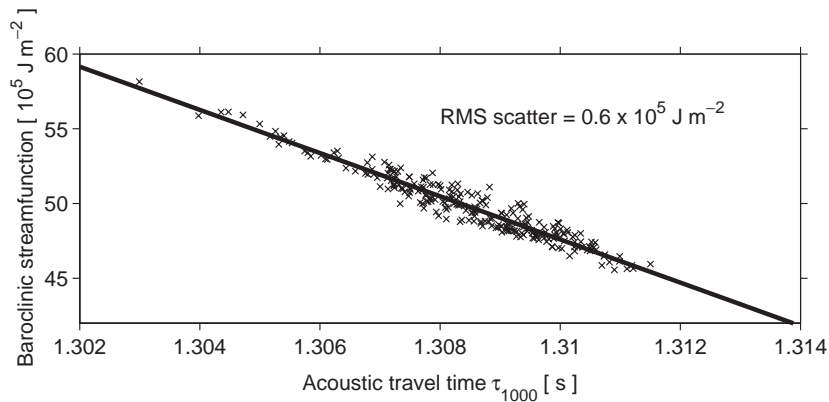


Fig. 3. Each symbol represents χ_{800} vs. τ_{1000} calculated with the T and S measurements of a single CTD; values for all 251 CTDs from the Abaco region are shown. Bold line represents a least-squares linear fit to the data. RMS difference from linear fit values indicated on plot.

that level). This calibration was completed in the same manner as the τ_{3000} calibration discussed above. Once calibrated in this manner, each of the IESs were combined with the slope and intercept from the linear fit in Fig. 3 to produce time series of χ_{800} at sites A, B, and D.

It should be noted that there are no technical reasons why the GEM field presented in Fig. 2 could not have been developed using τ_{1000} rather than τ_{3000} , which would allow all three IESs to utilize the GEM technique rather than just sites B and D. There are, however, several practical reasons why this was not done. The main consideration is noise reduction. The choice of the maximum pressure for the simulated τ integrations represents a balance between maximizing the number of CTDs from the region which can be used in building the GEM fields (only those CTDs reaching the maximum pressure can be used), while choosing a maximum depth encompassing as much of the baroclinic structure as possible (Meinen and Watts, 2000). Because there is still appreciable shear below 1000 dbar in the Abaco region, using τ_{1000} as the abscissa for the GEM fields would result in larger scatter about the GEM field. Of course, this additional scatter is also present in the single parameter correlations such as that shown in Fig. 3. Values of χ , however, represent a vertical integration quantity rather than a point value like T on a particular p surface,

and therefore the scatter can be lessened by an approach such as that shown in Fig. 3. Given the small size of the dynamic signals available in the Abaco region (full scale τ range of 12 ms compared to 55 ms for the North Atlantic Current for example, see Meinen and Watts, 2000), this increased scatter about the GEM fields is unacceptable. As a result the GEM approach was only applied to the deep IESs (sites B and D), providing detailed vertical structure information at those sites, while the χ method is applied to all three IESs for studying the shallow transport.

4. Results

By combining the calibrated IES τ time series with the T GEM field a time series of full water column profiles of temperature is obtained at site B and another time series is obtained at site D. The mean structures of temperature and salinity at sites B and D, as estimated by the IES–GEM observations, are presented in Fig. 4 to illustrate typical T and S values for this region. These time-mean temperatures agree well with those of the moored current meters; the CMMs did not have salinity sensors against which the IES–GEM estimates could be compared.

Some of the current meters on the moorings were equipped with pressure gauges (1200 dbar at

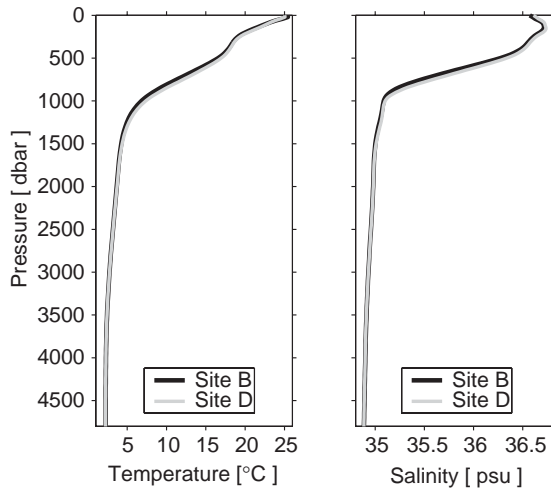


Fig. 4. Time-mean vertical structure of T and S determined from the IESs. Left panel shows the mean T profiles at sites B and D, right panel shows the mean S profiles.

site B and 800 and 1200 dbar at site D), which measure the ‘blow-over’ of the moorings as they are deflected by the currents. These pressure excursions can be quite large, exceeding a few hundred dbar at times. Following these pressure gauges up and down in the water column, the coincident T from the IES–GEM time series of T profiles is extracted to yield a time series of T . The comparisons of the directly measured temperatures from the moorings to those estimated by this IES–GEM combination are generally good (Fig. 5), with correlation coefficients ranging from 0.81 to 0.89. There are some consistent small biases of about 0.2°C for all three comparisons, however the differences are well within the estimated error bars (see Fig. 2, middle panel). Furthermore, because the small biases are of the same sign and roughly the same magnitude they will have little to no effect on the calculated velocities, which depend on density gradients between two points. It is clear, nonetheless, that the IES–GEM combination is picking up most of the variability observed by these three moored temperature sensors.

Similar comparisons could not be made for the deeper temperature gauges because none of those sensors had pressure gauges alongside. Nevertheless, by making some assumptions regarding

mooring motion at deeper levels based on that observed at 800 and 1200 dbar, or by applying a mooring design program to estimate mooring motion at these deeper instruments, a rough comparison can also be made of the deep temperature records to those estimated by the IES–GEM combination (not shown). For instruments moored at and below 2000 dbar such comparisons reveal root-mean-square (RMS) differences equal in magnitude to the observed temperature signals, indicating that the IES–GEM technique provides no skill in determining the temperatures at these depths and cannot observe small T changes such as those which herald the arrival of recently ventilated Labrador Sea Water (Molinari et al., 1998). This is consistent with the roughly 1-1 signal-to-noise ratio observed in the GEM field at those depths (Fig. 2, lower panel). The temperature variations are very small at these depths ($\leq 0.2^{\circ}\text{C}$) relative to the upper ocean temperature changes ($\geq 2^{\circ}\text{C}$), but a similar magnitude difference between upper ocean signal and deep ocean signal is also present in regions of the world ocean where the GEM technique has shown much stronger predictive ability in the deep ocean (e.g. Meinen and Watts, 2000). This lack of correlation between deep temperature variability and τ suggests that the deep temperature fluctuations in the Abaco area are not correlated with changes in the thermocline layer. Because the temperature variations in the upper ocean are much larger than those in the deep ocean, and because the IES measurement of τ is an integral measurement, these uncorrelated T signals at depth cannot be extracted from a signal dominated by the upper ocean signal. Instead they in essence manifest as enhanced scatter about the GEM field (lower panels in Fig. 2). As will now be shown, however, this does not imply that the IES–GEM combination cannot provide reasonably accurate velocity information at depth, because geostrophic velocities are also integral quantities (being proportional to geopotential anomaly gradients).

4.1. Test of IES–GEM for DWBC application

This study represents the first attempt to apply the GEM technique to IES data for the purpose of

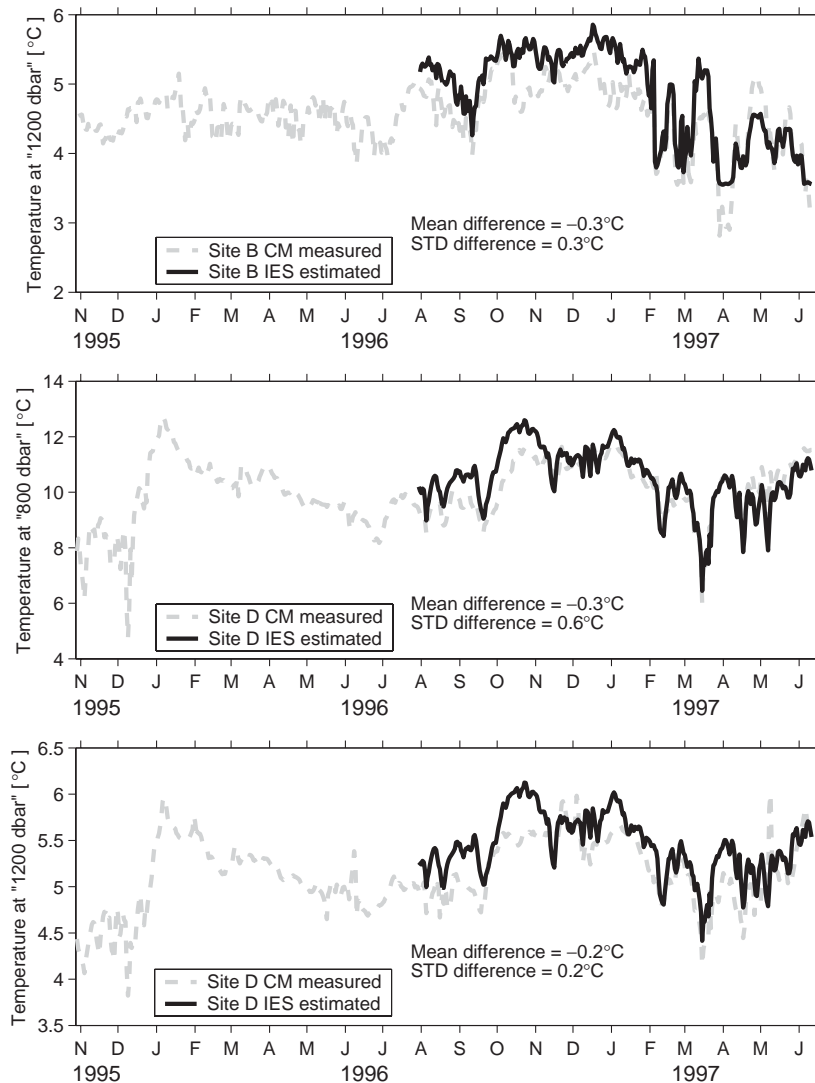


Fig. 5. Comparison of directly measured temperatures from instruments on moorings to the estimated temperature at the same levels from the IES–GEM combination. Comparisons are only shown for temperature gauges which were collocated with pressure gauges, so that the temperature at the same pressure could be extracted from the IES–GEM full water column temperature profiles. Upper, middle, and lower panels show the comparisons for the moored T and p instrument pairs at nominal depths of 1200 dbar at site B as well as 800 and 1200 dbar at site D, respectively. Mean and standard deviations of the differences (CMM–IES) during the coincident time periods are noted on each panel.

interpreting a deep ocean current (the DWBC), as opposed to an upper ocean current (e.g. Fig. 7 of Meinen and Watts, 2000). Therefore a series of comparisons between the velocity estimates from the IES–GEM data to direct measurements from the CMMs deployed during the study will be presented next.

Differencing the Φ profiles at sites B and D results in a time series of estimates of the geostrophic relative velocity perpendicular to the line between sites B and D. The relative velocities cannot be directly compared to observations from current meters, because a current meter measures absolute velocity. If there is more than one current

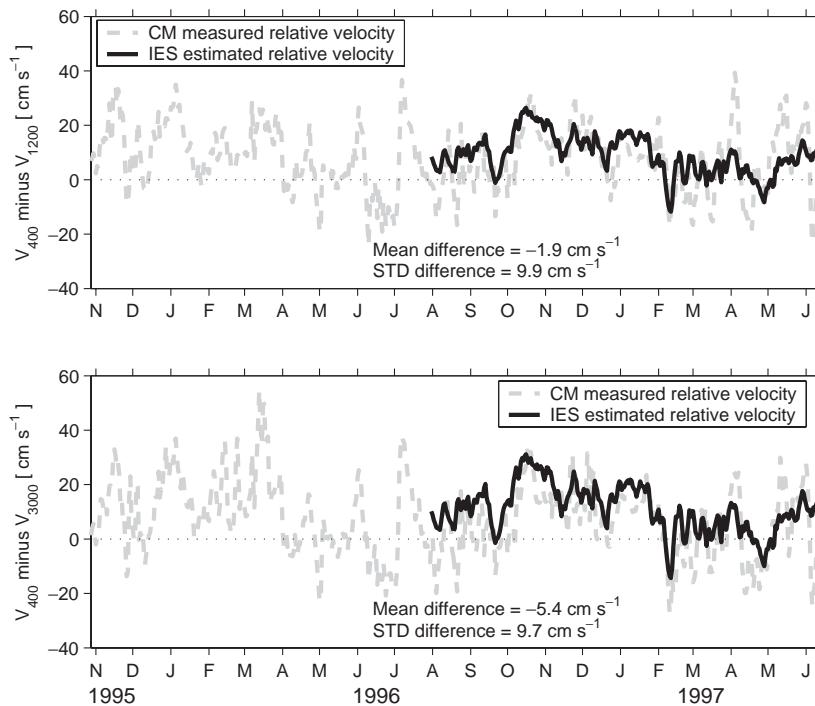


Fig. 6. Comparison of directly measured velocities from instruments on moorings to the estimated velocities from the IES–GEM combination. Comparisons are of relative velocities; current meters moored at the indicated two nominal pressure levels (e.g. 400 and 1200 dbar for upper panel) were differenced to provide the gray dashed lines, while IES–GEM estimated relative velocities were recalculated between the pressures measured coincident to the moored current meters. The 3000 dbar current meter was assumed not to blow over. Mean and standard deviation of the differences (CMM–IES) are noted in the panels.

meter on a mooring, however, and if the pressures at which both current meters reside are known, the two current meter records can be differenced to provide a relative velocity time series between moving pressure surfaces. The relative velocities derived from the IESs can then be reevaluated between the same two pressures and compared to the current meter measurements.

The current meters at nominal depths of 400 and 1200 m on the mooring at site C, located at the midpoint between the IESs at sites B and D, were both equipped with pressure gauges. The deeper current meters were not equipped with pressure gauges. Because moorings tend to blow over in such a way that the deeper instruments blow over less than those higher on the mooring, and because the velocity shear at great depth is generally very small, it was assumed for simplicity that the 3000 m current meter did not blow over during

the study. The velocities measured by the current meters nominally moored at 1200 and 3000 m were separately differenced with the velocity measured by the current meter at a nominal depth of 400 dbar at site C to yield to relative velocity profiles; one over 400–1200 dbar and the other over 400–3000 dbar. IES relative velocity time series were extracted over the same pressure range (where the level movements matched those from the moored pressure gauges) and were compared to the current meter measurements (Fig. 6). The RMS differences between the current meter measured time series and the IES–GEM estimated time series are quite small and the variability seems to agree well (correlation coefficients of 0.63 and 0.78 for 10 day averages of the velocities shown in the upper and lower panels of Fig. 6, respectively). Even in the absence of measurement errors and methodological problems, one would not expect

the agreement between these two velocities to be perfect because the current meters measure velocity at a discrete point while the IES–GEM derived velocities represent an average geostrophic velocity across the gap between sites B and D. The current meters will observe velocity changes due to much smaller scale oceanic features (both temporal and spatial) than the geostrophic velocity between the IESs. As such, the agreement between the time series shown in Fig. 6 is quite good. The surface flows in the gap between sites B and D have been shown previously to be fairly small in the mean (e.g. Leaman and Harris, 1990; Lee et al., 1996; Johns et al., 1997). This suggests that while the IES–GEM combination may not be able to observe the small temperature variations that occur in the deep ocean off Abaco, the technique does capture the majority of the velocity variations occurring at depths which correspond to the DWBC. The ability to capture the velocity, but not the deep temperature variations, results from the fact that the velocity is an integral quantity (proportional to gradients in Φ , which has been integrated from the surface to 3000 m for example), while temperature is a point measurement, and from the fact that the signal-to-noise ratio of the integrated Φ values is sufficiently good that the velocity shear through the upper portion of the DWBC is well estimated.

4.2. Mean vertical structure in the DWBC

Fig. 7 shows the time-mean geostrophic velocity structure relative to 800 dbar from the IES and GEM data; the cross-hatched region represents plus or minus one standard deviation of the temporal variability. The velocity structure agrees fairly well with the current meters, although the current meters indicate a more significant 5 cm s^{-1} reduction in meridional flow at the base of the DWBC between 2000 and 4500 dbar (Johns et al., submitted for publication), while the IES–GEM has a reduction of less than 1 cm s^{-1} between 3000 and 4500 dbar. Geostrophic velocities determined from the moored temperature sensors at sites B and D (applying historical T – S data to get density from T and to interpolate–extrapolate from a few sensors to a full-water-column profile of T) also

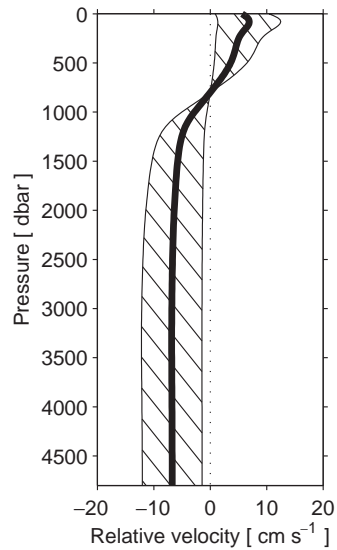


Fig. 7. Time-mean vertical structure of geostrophic velocity determined from the IESs. The plot shows the mean velocity profile between sites B and D relative to a level of no motion at 800 dbar. Cross-hatched region illustrates plus-minus one standard deviation based on the observed temporal variability over the year of measurements.

indicate a stronger shear, about 3 cm s^{-1} , at the base of the DWBC (Johns et al., submitted for publication). This lack of vertical shear from the IES–GEM technique may result from the inability to capture the small temperature (and density) variability occurring below 2000 dbar because it is uncorrelated to the dominant thermocline variability. Note, however, that the current meters deployed as part of this study had widely varying mean vertical shears, with a difference larger than 10 cm s^{-1} between the 2000 and 4000 dbar mean meridional velocities measured at site B, but only a 2 cm s^{-1} difference between the same levels at sites C and D. Furthermore, the magnitude of the shear was highly variable over the 2 years that the moorings were deployed (Johns et al., submitted for publication). As such, some portion of the difference between the IES–GEM shear at the base of the DWBC and the current meter data may result purely from horizontal sampling issues. Taken at face value, a 5 cm s^{-1} shear difference might lead one to expect a transport bias of about 5 Sv vs. the IES 1 cm s^{-1} shear, however, it is

shown below that the effect of this shear difference on the calculated DWBC transports between sites B and D is in fact much smaller. This occurs because the IES/GEM technique tends to underestimate the vertical shear both above and below the core of the DWBC somewhat, leading to a compensation in transport differences.

4.3. DWBC transport

As noted earlier, the DWBC transport was defined as the meridional flow between 800 and 4800 dbar between sites B and D (Fig. 8a). Transport here is simply the integral of velocity through this layer multiplied by the distance between sites B and D (82 km). Both absolute

transport (using the deep pressure gradient reference) and baroclinic transport (relative to 800 dbar) were calculated (Fig. 8a), and they yield record-length-mean transports of -25 ± 9 and -20 ± 6 Sv, respectively (see appendix for derivation of the estimated error bars). The standard deviations of the absolute (relative) transport was 21 Sv (15 Sv). This mean absolute DWBC transport is somewhat smaller than the 30–40 Sv found in previous studies (Lee et al., 1990, 1996), perhaps because the entire DWBC was not captured in the gap between sites B and D. Assuming the velocity structure inshore of site B was the same as between sites B and D (see Fig. 1), an admittedly questionable assumption, an additional 5 Sv of southward flow could be contained within the

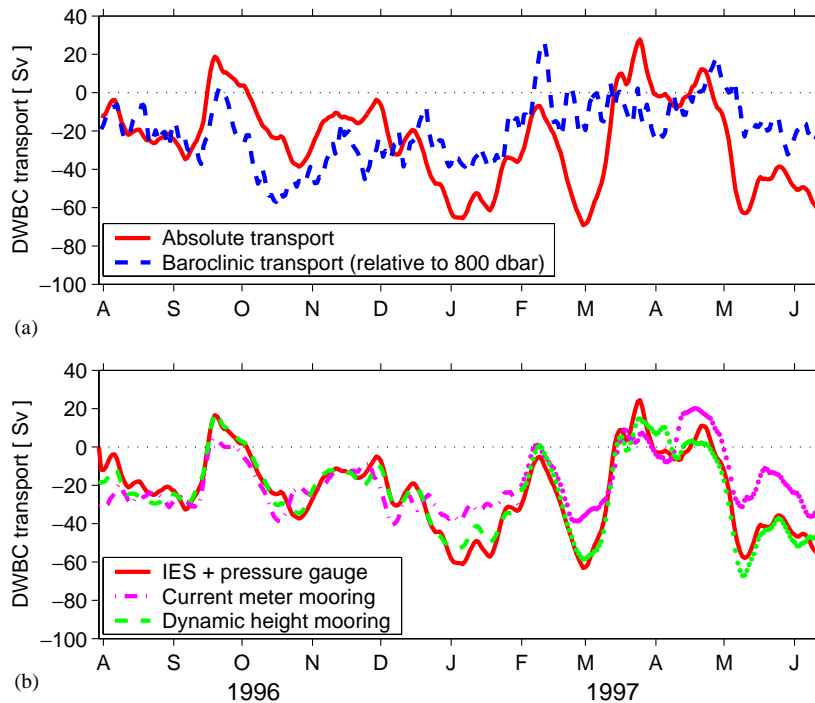


Fig. 8. Transport of the DWBC offshore of Abaco Island. (a) Baroclinic transport, relative to an assumed level of no motion at 800 dbar, and absolute transport integrated between 800 and 4800 dbar and between sites B and D. (b) Absolute transport from the IES combined with the bottom pressure measurements compared to absolute transport integrated from the observations of the coincident current meter line. Because current meter data was only available at 1200 dbar and below, the transports in this panel are integrated only over 1200–4800 dbar. Also shown is the transport determined by calculating dynamic heights from the temperature sensors moored alongside the current meters (Johns et al., submitted for publication), utilizing the same bottom pressure sensors for the barotropic reference as were used with the IES data. Current meter and dynamic height mooring estimates are dotted after February 1997 because after the loss of the upper portion of mooring B the remaining portion of the mooring flopped over, and it provided data over only a fraction of the DWBC layer. Units are Sverdrups ($1 \text{ Sv} = 10^6 \text{ m}^3 \text{ s}^{-1}$).

unobserved ‘bottom triangle’. The average of 11 PEGASUS sections at the same location in the mid 1980s found an additional 8 Sv of mean southward DWBC flow located inshore of site B integrated between 800 and 3000 dbar (Leaman and Harris, 1990). Wider arrays of current meters at 26.5°N, extending from mooring site A to site E, have also indicated a larger southward transport, about –27 Sv of absolute DWBC transport (Lee et al., 1996). As will be discussed shortly, however, the coincident current meter transport from this study integrated within the gap between sites B and D agrees quite well with the IES + bottom pressure gauge values. The periods of northward deep flow between sites B and D (e.g. September 1996, March–April 1997) are consistent with northward flow that has been observed when the DWBC meanders offshore (e.g. Hacker et al., 1996). Further complicating the DWBC transport picture is the presence of large recirculation cells which extend hundreds of kilometers into the interior (Johns et al., 1997).

It is evident when comparing the absolute and relative DWBC transports that, while the record-length-means might be similar, the variability of the two time series is completely different. The correlation coefficient between the two transport time series is only 0.33, indicating that a linear fit between the two would only explain 11% of the total variance. The most obvious result of this comparison, therefore, is that the use of a level of no motion assumption in trying to assess the DWBC transport from any individual CTD section will likely lead to a significant instantaneous error. The RMS difference between the two time series is 24 Sv, which is approximately equal to the time-mean absolute transport. The observed variability is difficult to assess in terms of actual DWBC variability, particularly the periods when the flow between 800 and 4800 dbar is *northward*, because it is impossible to determine whether the observed changes are due to the DWBC transport pulsing and changing (e.g. Chave et al., 1997) or whether the variability is due to the DWBC meandering into and out of the gap between sites B and D (e.g. Hacker et al., 1996; Lee et al., 1996).

The DWBC transport is strongly determined by the barotropic flow, where barotropic here has the

Fofonoff definition of near bottom velocity rather than being defined as a vertical average (Fofonoff, 1962). This is consistent with earlier mooring deployments in this area, which demonstrated the significant barotropic contribution to the DWBC flow (Lee et al., 1990). The pressure gauges provide the estimates of deep flow variability, which might suggest that the DWBC flow could be monitored with bottom pressure gauges alone. However, the variability of the relative transports is roughly 75% of the size of the variability of the absolute transport, indicating that the baroclinic changes observed by the IES–GEM method are not negligible.

A final test for the IES plus bottom pressure gauge method of determining the DWBC absolute transport is to compare it against a more ‘traditional’ measurement technique, the current meter moorings. Determining transport from a CMM array such as that deployed here (see Fig. 1) requires assumptions to account for mooring motion, for the extrapolation upward from the uppermost current meter on the moorings, and for the interpolation between mooring sites. The latter is the most worrisome in an array such as this, where the deep meridional currents are essentially uncorrelated between moorings B, C, and D ($r < 0.2$ for the 5-day running-mean data and $r < 0.6$ for 40-day running-mean data), indicating the current was undersampled for all but the longest time scales. Nevertheless, the current meter method is probably the most widely accepted standard for determining current transport, and as such it is the appropriate quantity to test the IES plus bottom pressure gauge method. Fig. 8b shows the absolute transport between 1200 and 4800 dbar (the widest depth range available from the current meters) integrated between sites B and D determined from the current meters at sites B, C, and D (Johns et al., submitted for publication) and compares it to the transport determined from the combined IES data and bottom pressure gauge data. The time series of current meter transport agrees fairly well with that from the IES plus pressure gauge; the RMS difference between the two time series is 12 Sv (time-mean offset 0.2 Sv) and the correlation coefficient is 0.76 for the 5-day running-mean data. This good agreement is

despite the fact that the IES–GEM method was failing to reproduce the proper shear at the base of the DWBC as discussed earlier.⁴ Given the ± 8 Sv absolute daily transport error bar estimated for the IES plus bottom pressure gauge method presented herein and the ± 8 Sv daily transport error bar estimated for the current meter integration (Johns et al., submitted for publication), the differences in transports are within the combined measurement accuracies of the two systems. Johns et al. (submitted for publication) also calculated transports for the same gap between sites B and D using dynamic heights calculated using the T measurements on the two moorings and canonical relationships between T and density. They referenced the resulting relative velocities with the same pressure gauges that were used for this study, however rather than use the 8.7 cm s^{-1} time-mean velocity from the 4000 m current meter on mooring C to provide the time-mean reference velocity they used the mean of two LADCP sections, which yielded a mean of 8 cm s^{-1} . The agreement between the “dynamic height mooring” transports and the IBS-based transports is excellent (Fig. 8b), with a mean offset of 0.5 Sv and a RMS difference of only 5 Sv. These differences are also well within the associated error bars for the two methods.

4.4. Antilles current (AC) transport

Using the linear relationship in Fig. 3, time series of Fofonoff potential χ (potential energy anomaly) integrated between the surface and 800 dbar were determined for each of the IESs at sites A, B, and D. Differences in χ between sites are proportional to the baroclinic transport above 800 dbar relative to 800 dbar. The differences in χ suggest that northward flow above 800 dbar occurs primarily between sites A and B, while the flow

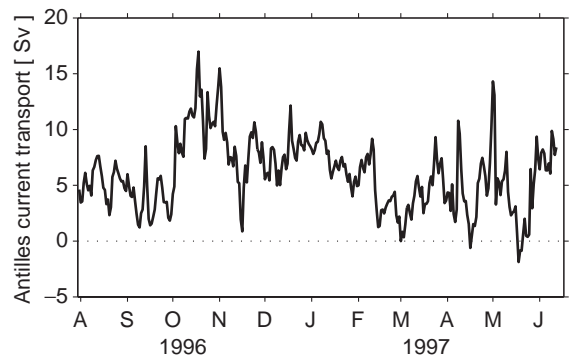


Fig. 9. Transport of the AC offshore of Abaco Island. Transport is baroclinic relative to an assumed level of no motion at 800 dbar and is integrated between the surface and 800 dbar. Values represent the transport between sites A and B (see Fig. 1), with the upper ocean transport between sites B and D also being added when the net upper ocean transport between those two sites was northward. Units are Sverdrups ($1 \text{ Sv} = 10^6 \text{ m}^3 \text{ s}^{-1}$).

between sites B and D is generally southward.⁵ This is consistent with the idea that the AC is trapped close to the top of the continental slope (Olson et al., 1984; Rosenfeld et al., 1989; Leaman and Harris, 1990). In periods when the upper ocean transport between sites B and D was northward, it is hypothesized that the AC has shifted enough away from the shelf to overwhelm the general weak southward flow typical for the upper ocean in this region (Leaman and Harris, 1990). Hence, the transport of the AC was defined here as the upper ocean transport between sites A and B, added to the upper ocean transport between sites B and D only during periods when the latter is northward (Fig. 9).

Based on the roughly 1 year of measurements obtained in this experiment, the time-mean AC transport (relative to an assumed level of no motion at 800 dbar) was $6.1 \pm 1.7 \text{ Sv}$ (see appendix for accuracy discussion). This is larger than a previous absolute transport estimate of about 5 Sv

⁴Note that in late January or early February the current meter mooring at site B lost its upper portion due to a wire separation. After this period the nominal 1200 m current meter on the mooring flopped over at times by as much as 900 dbar; the current meter transport integration is much less reliable after this point and therefore is denoted as a dotted line in Fig. 8b

⁵Two of the three current meters on mooring A failed, and mooring B lost its upper portion prior to recovery, so there is limited direct velocity data for comparison. The one functioning current meter on mooring A and the upper ocean current meters on mooring C are consistent in sign with the transports estimated from χ .

determined from a multi-year mooring deployment that observed the AC at the same site in the late 1980s and early 1990s using essentially one mooring (Lee et al., 1996). It also exceeds the 3.8 Sv absolute transport estimate from a series of 11 repeat snapshot PEGASUS sections which spanned a slightly longer 1985–1987 period (Leaman and Harris, 1990). These mean transport differences may reflect the inadequacy of the assumed 800 dbar level of no motion, or they may reflect sampling biases, however, the differences in mean transports are not statistically significant based on the estimated error bars. The AC transport observed during the study presented here was highly variable at time scales of a few days to a few months, with the strongest transport occurring in October–November 1996 and the weakest transports occurring over the period between March and May 1997. The standard deviation of the baroclinic transport was 3.2 Sv, while the individual daily values (after applying a 5 day running mean) are accurate to within about 2 Sv (including a possible 1.5 Sv bias, see appendix). The observed temporal variability is very similar to that observed from a series of 11 PEGASUS sections, which yielded a standard deviation of 3.9 Sv for the AC transport at 26.5°N (Leaman and Harris, 1990).

The AC is believed to be forced as part of the broad Sverdrup circulation (Olson et al., 1984), and as such it might be expected that the variations in AC transport might be correlated in some way with the variations in transport of the Florida Current to the west of Abaco Island at the same latitude. Comparison of the AC transport to the measured absolute transport of the Florida Current from the subsurface cable running from Florida to Grand Bahama Island (Baringer and Larsen, 2001) indicates that the two transport time series are not statistically correlated (not shown). This result is consistent with the PEGASUS section results of Rosenfeld et al. (1989), who also calculated transports for the Florida Current and AC in the mid-1980s and found that the currents were uncorrelated.

The AC time series does have similarities to the AC transport annual cycle observed in previous mooring experiments, which indicated minimums

in transport in March–April–May and September–October and maximums in November–December and June (Lee et al., 1996), however the agreement is not perfect. Perfect agreement is not expected, of course, due to the existence of mesoscale and interannual variability. The annual cycle only represents 9.7% of the total variance of the 1982–1998 Florida Current record, so any one year of Florida Current transport does not look much like its long-term mean annual cycle either. Longer deployments will be required to determine how much of the variability in AC transport is occurring at the annual and semi-annual periods associated with seasonal forcing in order to assess the importance of the apparent AC annual cycle differences relative to historical estimates.

5. Summary and conclusions

This study has examined a year-long deployment of IESs in the DWBC east of Abaco Island, the Bahamas, and has compared the inferred transports to a traditional CMM array. Historical hydrography and IES observations were used to quantify the baroclinic transport (relative to 800 dbar) associated with the northward flowing AC east of Abaco Island. The 11-month mean relative transport of about 6 Sv was a bit larger than previous absolute estimates of 4–5 Sv, however the differences are not statistically significant. Over the July 1995–June 1996 observation period there was no statistically significant correlation between the AC and the Florida Current transport observed to the west of Abaco Island in the Florida Straits (Baringer and Larsen, 2001), however the observed AC transports showed some similarities to previous estimates of the observed seasonal cycle in the AC (Lee et al., 1996).

IES data was combined with bottom pressure gauge observations and the deep mean velocity estimated from current meters to yield profiles of absolute velocity over the full water column. These velocity profiles were then used to estimate the absolute transport associated with the DWBC. The DWBC absolute transport (integrated between 800 and 4800 dbar) was highly variable, with the standard deviation (23 Sv) roughly equalling

the time series mean (-25 Sv). With only two IESs, it was not possible to determine what fraction of this variance was due to meandering of the DWBC into and out of the array (e.g. Hacker et al., 1996; Lee et al., 1996) as opposed to pulsation of the DWBC itself (Chave et al., 1997). The IES–GEM method for determining the vertical shear profile was unable to reproduce the deep velocity shear observed in current meter data at the base of the DWBC (Johns et al., submitted for publication), nonetheless this did not result in large errors in the IES+pressure gauge estimates of DWBC transport, with the two time series agreeing to within ± 12 Sv for transports integrated between 1200 and 4800 dbar. This is within the combined error bars for the two techniques. The CMM vs. IES+pressure gauge comparison indicated that the latter would allow for the monitoring of the DWBC transport variability at this location with about the same accuracy, but at a much lower cost, as a traditional “picket fence” of current meter moorings. As noted above, however, the deep vertical velocity structure would be less well determined by the IES+pressure gauge technique. Application elsewhere would require similar tests to those presented herein in order to validate the accuracy of this method for estimating deep transports at that location. A line of IESs with pressure gauges, commonly referred to as PIES, with occasional hydrographic cruises (every 1–2 years), represents a cost effective method for monitoring changes in the DWBC transport east of Abaco over longer time scales than has been possible in the past.

Acknowledgements

The authors would like to thank the following people who were involved in collecting, calibrating, and processing the hydrography and mooring data used in this study: E. Johns, T. Kanzow, T. Lee, R. Molinari, W.D. Wilson, Q. Yao, and R. Zantopp. This work would not have been possible without the excellent work of the crew and officers of the NOAA Ship Malcolm Baldrige and the NOAA Ship Ronald H. Brown and we heartily appreciate their help. G. Goni and the anonymous reviewers provided a number of helpful comments

for improving this manuscript. C. Meinen was funded for this work under the auspices of the Cooperative Institute for Marine and Atmospheric Studies (CIMAS), a joint institute of the University of Miami and the National Oceanic and Atmospheric Administration (NOAA), Cooperative Agreement #NA67RJ0149. S. Garzoli and M. Baringer were funded by NOAA, and the IES deployment was funded by NOAA/AOML. W. Johns and the CMM deployment was funded by NSF Grant OCE-9811374, and by NOAA Grant NA37RJ0200 administered through CIMAS.

Appendix A. Transport error analysis

A.1. AC transport accuracy

IESs and the GEM technique on their own only provide geostrophic velocities relative to an assumed level of no motion. As such, transports errors can result from errors in the IES–GEM estimates and from errors due to the assumed level of no motion. Without additional information from other observations it is impossible to estimate the error due to the level of no motion assumption, and therefore the accuracy discussion here must focus only on the accuracy of the *baroclinic* AC transport estimates. The errors in the AC baroclinic transport estimate result from the accuracy of the IES measured τ , the accuracy of the calibration of the IES measurements into τ_{1000} , and the scatter about the linear relationship in Fig. 3. The accuracy of the IES hourly measurement is roughly 1 ms (Chaplin and Watts, 1984; Meinen and Watts, 1998), which when combined with the slope from Fig. 3 yields a χ accuracy of $\pm 1.4 \times 10^5 \text{ J m}^{-2}$.

The calibration of the IES measured τ into τ_{1000} is susceptible to three sources of error; the error in assuming the magnitudes of τ variations are the same at 1000 dbar and at the pressure of the IES, the error in the CTD calculated τ_{1000} , and the errors in combining the CTD simulated τ_{1000} with the temporally coincident τ measurement from the IES. The first two can be estimated using hydrographic data, while the third can be estimated by looking at the temporal variability of the IES

measurements over a 4–5 h period. The three sources result in potential errors of 0.5, 0.1, and 0.5 ms, respectively. Combining the three sources of error which contribute to the conversion of τ_{IES} into τ_{1000} in a square-root of the sum of squares manner yields an accuracy of 0.7 ms, which corresponds to a χ accuracy of $\pm 1.0 \times 10^5 \text{ J m}^{-2}$.

The scatter about the linear relationship in Fig. 3 could introduce an error of $\pm 0.6 \times 10^5 \text{ J m}^{-2}$. This error is independent from the τ calibration and τ measurement errors, and so the total error in the IES estimated χ is the square root of the sum of the squares of the individual errors, which is $1.8 \times 10^5 \text{ J m}^{-2}$. The transport estimates presented herein result from the difference in χ at two sites scaled by density and the Coriolis parameter (Fofonoff, 1962); the error in such a difference would be at most $\sqrt{2}$ times the error in χ at one end, assuming they are independent errors, scaled by density and the Coriolis parameter. Using a value of 1030 kg m^{-3} for density and $6.5 \times 10^{-5} \text{ s}^{-1}$ for the Coriolis parameter, the resulting accuracy of an hourly estimate of the baroclinic transport between two IESs is about 4 Sv. Most of these potential sources of error are random in nature; only the error resulting from using the CTD estimated τ_{1000} to determine the mean offset from τ_{IES} is a bias, and that error could be reduced with multiple calibration CTDs if they were available. While this estimated accuracy bound seems quite large compared to the AC transports shown in Fig. 9, representing about 120% of the observed standard deviation of the transport over the full record, note that this is an accuracy for the *hourly* transport estimates. Separating out the random and bias errors, and taking into account the 40 h boxcar filter and the 5 day running mean, the daily AC baroclinic transports presented herein are accurate to within about 2 Sv. With an average integral time scale (Emery and Thomson, 1997) of 13 days from the IES records, the full records yield about 12 degrees of freedom. So the measurement accuracy contribution to the error bar for the time-mean AC transport is essentially equal to the bias error of 1.5 Sv. The statistical standard error of the mean (Emery and Thomson, 1997) is about 0.9 Sv, so the total combined measurement and statistical error bar for the AC baroclinic transport is 1.7 Sv.

A.2. DWBC transport accuracy

The DWBC transport was estimated using a GEM approach, however, a similar approach to the AC error analysis can be applied. The IES measurement error and IES calibration errors are the same for both methods, the only difference would be a new calculation for the scatter around relationship between the CTD simulated τ values (in this case τ_{3000} rather than τ_{1000}) vs. χ . The RMS scatter about the χ_{4000} vs. τ_{3000} linear fit (not shown) is about $4.4 \times 10^5 \text{ J m}^{-2}$. Combining this with the other error sources, the baroclinic full water column hourly sample transport accuracy was roughly $\pm 9 \text{ Sv}$. The daily estimates of DWBC baroclinic transport, after the application of the 40 h boxcar filter and the 5 day running mean, is 2.6 Sv (2.2 Sv random scatter, 1.5 Sv potential bias).

Finally, the barotropic transport of the DWBC is based on the pressure gauges (for the time-varying component) and the deep current meters (for the time mean). The accuracy of using the point measurement current meter record at site C to provide an estimate for the horizontally integrated deep time-mean velocity between sites B and D is difficult to explicitly determine, however a reasonable estimate would be to look at the differences between the deep mean velocities at moorings B, C, and D. The average difference between the three deep time-mean meridional velocities and their mutual average was about 2 cm s^{-1} , which is also the average of the three statistical standard errors of the mean. This corresponds to a potential transport bias of as large as 8 Sv.

The accuracy of the pressure gauges has two components; the precision of the instantaneous pressure measurement and the accuracy of drift removal. The precision of the deep pressure gauges is 0.001 dbar according to the manufacture specifications; assuming the errors were of equal magnitude at sites B and D and that the errors were independent of one another this translates to an error in the deep velocity of about 0.2 cm s^{-1} . The second component of the pressure accuracy relates to how well the long-term drift can be removed from the record (Watts and

Kontoyiannis, 1990). Pressure sensors tend to exhibit long-period exponential drifts that can only be removed to within an accuracy of about 0.015 dbar, which would correspond to a velocity error of about 3.9 cm s^{-1} . This error applies only at the longest time scales, periods greater than 100 days (Watts and Kontoyiannis, 1990), and is largest during the initial few months of the record. Because the pressure gauges used herein had been in the water for a full year prior to the IES deployment, this source of error will be neglected in the error analysis. With 82 km between sites B and D, and with a DWBC layer thickness of approximately 3600 m, the combined errors correspond to an hourly absolute barotropic transport accuracy of 8 Sv (1 Sv random scatter from the pressure gauge precision, 8 Sv potential bias from the accuracy of the time-mean current meter estimate). If the same number of degrees of freedom are obtained in the barotropic signals as were in the baroclinic signals, the daily barotropic transport accuracy after the application of the 5 day running mean is 8 Sv (< 1 Sv random scatter, 8 Sv potential bias).

The absolute DWBC transport accuracy will be a combination of the barotropic and baroclinic components, in a square-root of the sum of squares sense because the two errors are independent. As such, the daily absolute DWBC transport, after the application of the 5 day running mean, should be accurate to within 8 Sv (2 Sv random scatter, 8 Sv potential bias). The time mean DWBC transport measurement accuracy, again assuming the same number of degrees of freedom as were determined from the IESs, would be 8 Sv (1 Sv random scatter, 8 Sv potential bias). The statistical standard error of the mean is 5 Sv, so the total accuracy (statistical plus measurement) of the time-mean absolute DWBC transport is about 9 Sv.

References

- Baringer, M.O., Larsen, J.C., 2001. Sixteen years of Florida current transport at 27°N . *Geophysical Research Letters* 28 (16), 3179–3182.
- Book, J.W., Wimbush, M., Imawaki, S., Ichikawa, H., Uchida, H., Kinoshita, H., 2002. Kuroshio temporal and spatial variations south of Japan determined from inverted echo sounder measurements. *Journal of Geophysical Research* 107 (C9), 3121 (doi:10.1029/2001JC000795).
- Chaplin, G.F., Watts, D.R., 1984. Inverted echo sounder development. In: *IEEE Oceans '84 Conference Record*, vol. 1, pp. 249–253.
- Chave, A.D., Luther, D.S., Filloux, J.H., 1997. Observations of the boundary current system at 26.5°N in the subtropical North Atlantic Ocean. *Journal of Physical Oceanography* 27 (9), 1827–1848.
- Del Grosso, V.A., 1974. New equation for the speed of sound in natural waters (with comparisons to other equations). *Journal Acoustical Society of America* 56 (4), 1084–1091.
- Dickson, B., Yashayaev, I., Meincke, J., Turrell, B., Dye, S., Holfort, J., 2002. Rapid freshening of the deep North Atlantic Ocean over the past four decades. *Nature* 416 (6883), 832–837.
- Emery, W.J., Thomson, R.E., 1997. *Data Analysis Methods in Physical Oceanography*. Pergamon Press, Oxford.
- Fischer, J., Schott, F.A., 1997. Seasonal transport variability of the deep western boundary current in the equatorial Atlantic. *Journal of Geophysical Research* 102 (C13), 27,751–27,769.
- Fischer, J., Schott, F.A., 2002. Labrador sea water tracked by profiling floats—from the boundary current into the open North Atlantic. *Journal of Physical Oceanography* 32 (2), 573–584.
- Fofonoff, N.P., 1962. Dynamics of ocean currents. In: Hill, M.N. (Ed.), *The Sea: Ideas and observations on Progress in the Study of the Seas*, vol. 1. *Physical Oceanography*, Wiley/Interscience, New York, pp. 323–395.
- Hacker, P., Firing, E., Wilson, W.D., Molinari, R., 1996. Direct observations of the current structure east of the Bahamas. *Geophysical Research Letters* 23 (10), 1127–1130.
- Johns, E., Fine, R.A., Molinari, R.L., 1997. Deep flow along the western boundary south of the Blake Bahama Outer Ridge. *Journal of Physical Oceanography* 27 (10), 2187–2208.
- Johns, W.E., Kanzow, T., Zantopp, R. Volume transports from dynamic height and current meters east of Abaco. *Deep-Sea Research I*, submitted for publication.
- Leaman, K.D., Harris, J.E., 1990. On the average absolute transport of the deep western boundary currents east of Abaco Island, the Bahamas. *Journal of Physical Oceanography* 20 (3), 467–475.
- Lee, T.N., Johns, W., Schott, F., Zantopp, R., 1990. Western boundary current structure and variability east of Abaco, Bahamas at 26.5°N . *Journal of Physical Oceanography* 20 (3), 446–466.
- Lee, T.N., Johns, W.E., Zantopp, R.J., Fillenbaum, E.R., 1996. Moored observations of western boundary current variability and thermohaline circulation at 26.5°N in the subtropical North Atlantic. *Journal of Physical Oceanography* 26 (6), 962–983.
- Meinen, C.S., Luther, D.S., 2003. Comparison of methods of estimating mean synoptic current structure in “stream coordinates” reference frames with an example from the

- Antarctic Circumpolar Current. *Deep-Sea Research I* 50 (2), 201–220.
- Meinen, C.S., Watts, D.R., 1998. Calibrating inverted echo sounders equipped with pressure sensors. *Journal of Atmospheric and Oceanic Technology* 15 (6), 1339–1345.
- Meinen, C.S., Watts, D.R., 2000. Vertical structure and transport on a transect across the North Atlantic Current near 42°N: time series and mean. *Journal of Geophysical Research* 105 (C9), 21,869–21,891.
- Meinen, C.S., Luther, D.S., Watts, D.R., Tracey, K.L., Chave, A.D., Richman, J., 2002. Combining inverted echo sounder and horizontal electric field recorder measurements to obtain absolute velocity profiles. *Journal of Atmospheric and Oceanic Technology* 19 (10), 1653–1664.
- Molinari, R.L., Fine, R.A., Wilson, W.D., Curry, R.G., Abell, J., McCartney, M.S., 1998. The arrival of recently formed Labrador sea water in the deep western boundary current at 26.5°N. *Geophysical Research Letters* 25 (13), 2249–2252.
- Olson, D.B., Schott, F.A., Zantopp, R.J., Leaman, K.D., 1984. The mean circulation east of the Bahamas as determined from a recent measurement program and historical XBT data. *Journal of Physical Oceanography* 14 (9), 1470–1487.
- Pickart, R.S., 1994. Interaction of the Gulf stream and deep western boundary current where they cross. *Journal of Geophysical Research* 99 (C12), 25,155–25,164.
- Rhein, M., Fischer, J., Smethie Jr., W.M., Smythe-Wright, D., Weiss, R.F., Mertens, C., Min, D.-H., Fleischmann, U., Putzka, A., 2002. Labrador sea water: pathways, CFC inventory, and formation rates. *Journal of Physical Oceanography* 32 (2), 648–665.
- Rosenfeld, L.K., Molinari, R.L., Leaman, K.D., 1989. Observed and modeled annual cycle of transport in the straits of Florida and east of Abaco Island, the Bahamas (26.5°N). *Journal of Geophysical Research* 94 (C4), 4867–4878.
- Rossby, T., 1969. On monitoring depth variations of the main thermocline acoustically. *Journal of Geophysical Research* 74 (23), 5542–5546.
- Schott, F.A., Zantopp, R., Stramma, L., Dengler, M., Fischer, J., Wibaux, M., 2004. Circulation and deep water export at the western exit of the subpolar North Atlantic. *Journal of Physical Oceanography* 34 (4), 817–843.
- Smethie Jr., W.M., Fine, R.A., Putzka, A., Jones, E.P., 2000. Tracing the flow of North Atlantic deep water using chlorofluorocarbons. *Journal of Geophysical Research* 105 (C6), 14,297–14,323.
- Smith, W.H.F., Sandwell, D.T., 1997. Global sea floor topography from satellite altimetry and ship depth soundings. *Science* 277 (5334), 1956–1962.
- Sun, C., Watts, D.R., 2002. Heat flux carried by the Antarctic circumpolar current mean flow. *Journal of Geophysical Research* 107 (C9), 3119 (doi:10.1029/2001JC001187).
- Watts, D.R., Kontoyiannis, H., 1990. Deep-ocean bottom pressure measurement: drift removal and performance. *Journal of Atmospheric and Oceanic Technology* 7 (2), 296–306.
- Watts, D.R., Rossby, H.T., 1977. Measuring dynamic heights with inverted echo sounders: results from MODE. *Journal of Physical Oceanography* (3), 345–358.
- Watts, D.R., Tracey, K.L., Bane, J.M., Shay, T.J., 1995. Gulf stream path and thermocline structure near 74°W and 68°W. *Journal of Geophysical Research* 100 (C9), 18,291–18,312.
- Watts, D.R., Qian, X., Tracey, K.L., 2001a. Mapping abyssal current and pressure fields under the meandering Gulf stream. *Journal of Atmospheric and Oceanic Technology* 18 (6), 1052–1067.
- Watts, D.R., Sun, C., Rintoul, S., 2001b. A two-dimensional gravest empirical mode determined from hydrographic observations in the subantarctic front. *Journal of Physical Oceanography* 31 (8), 2186–2209.
- Zantopp, R.J., Lee, T.N., Johns, W.E., 1998. Moored current meter observations east of Abaco, The Bahamas (“ACCP-3” array). Technical Report 98-006, Rosenstiel School of Marine and Atmospheric Science, University of Miami, Miami, FL.